Klover Multidisciplinary Journal of Engineering
Volume 10 Issue 1, January-March 2022
ISSN: 2995-4118
Impact Factor: 6.40
http://kloverjournals.org/journals/index.php/Engineering

DEEP KOOPMAN NEURAL NETWORKS FOR NONLINEAR PROCESS MONITORING IN STOCHASTIC PRODUCTION SYSTEMS

Song, Yu-Jie and Ma, Jian-Guo
East China University of Science and Technology, Shanghai, China

Abstract
Stochastic production systems (SPS) play a pivotal role in industries such as fermentation, pharmaceuticals, and composite material production, where stringent quality constraints are paramount. To ensure product quality in such systems, effective process monitoring is imperative. However, SPS presents significant challenges due to its inherent stochasticity and measurement uncertainties, stemming from sensitivity to exogenous factors and the lack of accurate in-situ measurements. This paper explores the landscape of SPS process monitoring methods, highlighting their limitations and proposing a novel approach leveraging recurrent neural networks (RNNs), particularly Long Short-Term Memory (LSTM) networks.

Keywords: Stochastic production system, process monitoring, recurrent neural networks, Long Short-Term Memory, quality constraints.

Introduction:

Stochastic production systems (SPS) have found applications in diverse fields, including fermentation, pharmaceuticals, and composite material production [1]-[7]. These applications demand stringent quality control measures to ensure the desired product quality. However, SPS presents unique challenges for process monitoring due to its inherent stochastic nature and measurement uncertainties, making effective quality control a complex endeavor. This introduction sets the stage for the exploration of process monitoring methods in SPS, emphasizing the need for innovative approaches.

SPS exhibits significant intrinsic stochasticity, primarily attributed to its sensitivity to various exogenous factors such as input variations, environmental conditions, and equipment status. These factors can introduce substantial variability in the quality and performance of the final product. Moreover, the lack of accurate in-situ measurement methods adds an extra layer of noise to the available data, making process monitoring in SPS indispensable yet inherently challenging.

Over the past few decades, researchers have developed several methods for SPS process monitoring. One prevalent approach is the application of multiway Principal Component Analysis (PCA) [8]. While this method offers simplicity, low-dimensional computation, and fast processing of high-dimensional data, it is inherently linear and struggles to capture nonlinear dynamics—a prevalent feature in SPS.

To address the limitations of linear methods, researchers have explored kernel methods, which map data into high-dimensional feature spaces where linearity can be preserved [9]. Additionally, there have been efforts to enhance Independent Component Analysis (ICA) methods [10], propose novel strategies like the kernel ICAPCA method [11], and develop multiway kernel entropy ICA methods [12]. These approaches aim to capture the nonlinear and non-Gaussian characteristics inherent in SPS data.

Furthermore, Support Vector Machines (SVM) integrated with PCA or fuzzy reasoning have been employed for anomaly detection in SPS [13], [14]. However, these methods have limited capacity to handle heavy-tailed and multimodal SPS data, and their hyperparameter tuning can be cumbersome.
The universal approximation theorem underscores the potential of neural networks to represent any function between inputs and outputs [15], making them an attractive option for SPS process monitoring. Auto-associative neural networks [16], [17] and deep neural networks [18]-[22] have been extensively explored for this purpose. However, these methods often assume sample independence and overlook dynamic correlations, limiting their effectiveness in capturing the complexities of SPS data.
Recurrent neural networks (RNNs), particularly Long Short-Term Memory (LSTM) networks [23], offer a promising alternative for SPS process monitoring. LSTMs excel at predicting future system evolutions based on current and historical data, making them well-suited for anomaly detection [24], [25]. Nevertheless, their use is sometimes criticized for their limited interpretability, as they provide few insights into the underlying physical processes.
In this paper, we delve into the application of LSTM networks for SPS process monitoring, aiming to overcome the limitations of existing methods and provide a deeper understanding of the monitored systems. Our proposed approach leverages the predictive power of LSTMs while striving to enhance interpretability, ultimately contributing to more effective and insightful SPS process monitoring.

2. Problem Statement

The most representative example of SPS is biochemical systems, and hence we will focus on it to showcase the developed method in the rest of the paper. The essence of biochemical systems is to convert substrates into high-value-added metabolites by living organisms (mostly cells). One of the major impediments for biochemical system production in high quality and quantity stems from the existence of a subpopulation of cells showing remarkably reduced production efficiency and capacity, which is termed as population heterogeneity in synthetic biology [1]. Such heterogeneity is an inevitable consequence of stochastic gene expression, which is solidly supported by massive single-cell experiments [39], [40]. In the context of biochemistry, gene expression indeed consists of a set of biochemical reactions with the participation of various macromolecules harbored in microscopic reactors (cells). The scarce of such macromolecules and the random molecular collision in the crowding reaction compartment of limited volume collectively lead to the stochasticity of intracellular biochemical reaction, particularly gene expression. As such, it is plausible to focus on gene expression process, which is the most critical and representative part. Without any loss of generality, any intracellular biochemical reaction can be described by

$$\sum_{i=1}^{N} s_{ir} X_i \xrightarrow{k_r} \sum_{i=1}^{N} p_{ir} X_i, \quad r = 1, 2, \cdots, R, \tag{1}$$

where X_i stands for species i ($i = 1, 2, \cdots, N$), the stoichiometric coefficients s_{ir} and p_{ir} are nonnegative integers specifying the molecule numbers of reactants and products involved in reaction r respectively, and k_r is the rate constant of reaction r. In the stochastic sense, k_r is inversely proportional to the mean time of two successive reactions. The propensity of reaction is

$$f_r(\mathbf{n}) = k_r \Omega \prod_{i=1}^{N} \frac{n_i!}{(n_i - s_{ir})! \Omega^{s_{ir}}}, \tag{2}$$

Klover Multidisciplinary Journal of Engineering
Volume 10 Issue 1, January-March 2022
ISSN: 2995-4118
Impact Factor: 6.40
http://kloverjournals.org/journals/index.php/Engineering

with Ω being the compartment volume and n_i being the molecule number of reactant i. Indeed, the propensity can be loosely understood as the probability of reaction occurrence. For instance, the transcription can be compactly described by

$$G \xrightarrow{\rho} G + M, \quad (3)$$

where G, M stand for gene and messenger RNA (mRNA) respectively, and ρ is the transcription rate constant.

Besides, there are various exogenous factors perturbing the normal operation of biochemical system, such as temperature fluctuation and contamination. The temperature impacts the reaction through reaction constants according to Arrhenius law. Arguably, so is the mechanism of contamination, as contamination may affect the catalytic efficiency of some enzyme. Hence, within the framework, when an anomaly takes place, it is reflected through the change of one or a group of reaction rate constants $\overset{k_r}{X_i}$. The goal of process monitoring then becomes detecting anomaly from the data of reaction species if some reaction rate constant k_r changes.

3. Methods

3.1. Data Acquisition

The dynamics of system (1) can be simulated by the renowned Stochastic Simulation Algorithm (SSA), also known as Gillespie algorithm in systems biology [41]. The basic idea is to draw two random numbers, one for calculating the next reaction time, and the other for determining next reaction type. The pseudocode for SSA is presented as follows.

Algorithm 1 Stochastic Simulation Algorithm
1: **Initialization:** $t \leftarrow 0, \mathbf{n}, t_{max}$
2: **Repeat**
3: Calculate propensities according to (2)
4: Obtain the time step to the next reaction event $\tau = -\ln(u_1)/\lambda, \lambda = \sum_{r=1}^{R} f_r(\mathbf{n})$
5: Determine the next reaction event $r = \text{smallest integer satisfying} \sum_{i=1}^{r} f_i(\mathbf{n}) > u_2\lambda$
6: Update time $t \leftarrow t + \tau$
7: Update according to (1)
8: **Until** $t > t_{max}$
Output:

Notably, there is a Julia implementation developed by our group and available on Github as DelaySSAToolkit. The package is based on DiffEqJump, but more powerful as it is even able to simulate delayed reactions [42].

3.2. Koopman Operator Theory

Here we present a brief summary of Koopman operator theory. For more details, readers are encouraged to refer to [43]. Considering a discrete-time system, whose dynamics are governed by

$$\mathbf{x}_{k+1} = \mathbf{F}(\mathbf{x}_k). \quad (4)$$

The state $\mathbf{x}_k$ is only observable through some function φ such that

Klover Multidisciplinary Journal of Engineering
Volume 10 Issue 1, January-March 2022
ISSN: 2995-4118
Impact Factor: 6.40
http://kloverjournals.org/journals/index.php/Engineering

$$\mathbf{y}_k = \varphi(\mathbf{x}_k) = [\varphi_1(\mathbf{x}),\ \cdots,\ \varphi_n(\mathbf{x})]^\top. \quad (5)$$

As shown in Figure 1, the Koopman operator $\mathbf{K}$ is an infinite-dimensional linear operator acting on observing function φ such that

$$\mathbf{K}\varphi = \varphi \circ \mathbf{F} \Leftrightarrow \mathbf{K}\mathbf{y}_k = \mathbf{y}_{k+1}, \quad (6)$$

where $\circ$ is the composition operator.

Suppose that in some Hilbert space spanned by a set of basis functions ϕ_i termed Koopman eigenfunctions satisfying that

$$\phi_i(\mathbf{x}_{k+1}) = \mathbf{K}\phi(\mathbf{x}_k) = \lambda_i\phi(\mathbf{x}_k). \quad (7)$$

It follows that observing function can be compactly decomposed into

$$\varphi(\mathbf{x}) = \sum_{i=1}^{\infty} \phi_i(\mathbf{x})\mathbf{v}_i, \quad (8)$$

with the Koopman mode being $\mathbf{v}_i = [\langle\phi_i, \varphi_1\rangle, \cdots, \langle\phi_j, \varphi_n\rangle]^\top$. As per (7), the evolution of the measurement dynamics can be presented as

$$\varphi(\mathbf{x}_{k+1}) = \mathbf{K}\varphi(\mathbf{x}_k) = \sum_{i=1}^{\infty} \lambda_i\phi_i(\mathbf{x}_k)\mathbf{v}_i, \quad (9)$$

which is referred as Koopman mode decomposition and tightly connected to DMD. DMD is indeed a finite truncation of Koopman mode decomposition for a linear system (is a linear function) [28], [43].

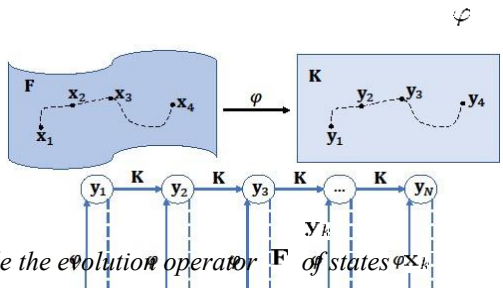

Figure 1: Schematic of Koopman operator theory. An observing function φ maps system states $\mathbf{x}_k$ into a high-dimensional space where measurements $\mathbf{y}_k$ evolving linearly governed by Koopman operator $\mathbf{K}$, *while the evolution operator* $\mathbf{F}$ *of states* $\mathbf{x}_k$ is usually nonlinear [43].

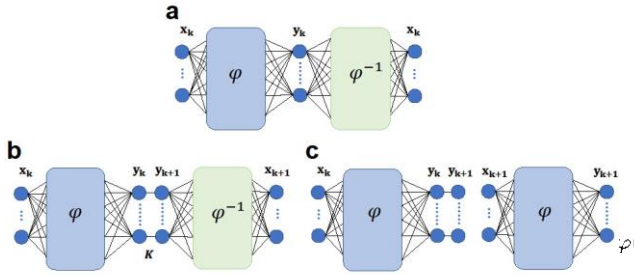

Figure 2: Schematics of deep Koopman neural network. (a) shows an autoencoder and establishing a bijective static mapping between the original space $\mathbf{x}_k$ and the high-dimensional linear space φ^{-1}. (b) shows how the DKNN performs one-step prediction. (c) interprets the loss function . The left panel corresponds to $\mathbf{K}\varphi(\mathbf{x}_k)$, while the right stands for .

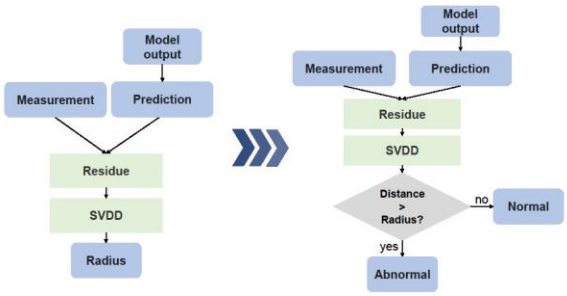

Klover Multidisciplinary Journal of Engineering
Volume 10 Issue 1, January-March 2022
ISSN: 2995-4118
Impact Factor: 6.40
http://kloverjournals.org/journals/index.php/Engineering

Figure 3: DKNN based anomaly detection protocol. Left: SVDD calculates the radius associated with 90% confidence interval based on the residues between predictions and measurements. Right: An anomaly is detected if the residue of a newly cast prediction is larger than an established radius. Otherwise, the system is still working in normal.

3.3. Deep Koopman Neural Network

KOT is a seemingly elegant theory enabling global linearization but rather difficult to perform, as solving the triplet of the eigenfunction ϕ_i, the eigenvalue λ_i and the mode $\mathbf{v}_i$ is a daunting task. The choice of eigenfunctions is non-trivial and calls for intricate tricks. In stark contrast, deep neural network provides a convenient way to seek the eigenfunctions. Reference [33] reported a neat approach based on a deep autoencoder which constitutes a bijective mapping between the original space and the highdimensional linear space and approximates the set of the valid eigenfunction bases (see Figure 2a). Note that [33] needs an auxiliary neural network to perform the Koopman operator, and it substantially increases the complexity. As such, we revise the neural network presented in [33] by removing the auxiliary neural network and identifying the linear operator $\mathbf{K}$ directly, which is modeled by a linear network (see Figure 2b). Subsequently, we specify the loss function for the DKNN training. The loss function is composed of five parts, the first three of which is specified as follows

$$\begin{aligned}\mathcal{L}_a &= \left\|\mathbf{x}_k - \varphi^{-1}\left(\varphi\left(\mathbf{x}_k\right)\right)\right\|_{\mathrm{MSE},}\\ \mathcal{L}_b &= \left\|\mathbf{x}_{k+1} - \varphi^{-1}\left(\mathbf{K}\varphi\left(\mathbf{x}_k\right)\right)\right\|_{\mathrm{MSE},}\\ \mathcal{L}_c &= \left\|\varphi\left(\mathbf{x}_{k+1}\right) - \mathbf{K}\varphi\left(\mathbf{x}_k\right)\right\|_{\mathrm{MSE}.}\end{aligned} \tag{10}$$

Here $\mathcal{L}_a$ and $\mathcal{L}_b$ represent the reconstruction error and one-step prediction error in the original space respectively, and $\mathcal{L}_c$ is the one-step prediction error in the high-dimensional linear space (see Figure 2c). The subscript MSE stands for mean squared error.

An $\mathcal{L}_\infty$ term is also used to penalize the data point with the largest loss

$$\begin{aligned}\mathcal{L}_\infty = &\left\|\mathbf{x}_k - \varphi^{-1}\left(\varphi\left(\mathbf{x}_k\right)\right)\right\|_\infty\\ &+ \left\|\mathbf{x}_{k+1} - \varphi^{-1}\left(\mathbf{K}\varphi\left(\mathbf{x}_k\right)\right)\right\|_{\infty}.\end{aligned} \tag{11}$$

Additionally, l_2 regularization is imposed on the neural network weights $\mathbf{W}$ to prevent overfitting

$$\mathcal{L}_{\mathbf{W}} = \|\mathbf{W}\|_2^2. \tag{12}$$

Hence, the total loss function is the weighted summation of all the five parts

$$\mathcal{L} = \alpha_1\mathcal{L}_{\mathrm{a}} + \alpha_2\mathcal{L}_{\mathrm{b}} + \alpha_3\mathcal{L}_{\mathrm{c}} + \alpha_4\mathcal{L}_\infty + \alpha_5\mathcal{L}_{\mathbf{W}}, \tag{13}$$

where for $i = 1, \ldots, 5$ stands for the weight for each parts in the loss function. The DKNN is then determined by solving the optimization problem $\min_{\mathbf{K},\mathbf{W},b}\mathcal{L}$. For SPS process monitoring, the input $\mathbf{x}_k$ can be the moments (mean, variance, etc.) of molecule counts of interest.

3.4. Anomaly Detection Protocol

With the DKNN model well trained, it is possible to calculate the residues between the model predictions and measurements. Given the residues yielded, the SVDD is used to compute the 90% confidence threshold, which is termed as radius thereafter (see Figure 3Left). In practice, given the historical data, DKNN casts one-step predictions, which are used to compute the residues. The yielded

Klover Multidisciplinary Journal of Engineering
Volume 10 Issue 1, January-March 2022
ISSN: 2995-4118
Impact Factor: 6.40
http://kloverjournals.org/journals/index.php/Engineering

residues are compared with the radius obtained before. If a residue is larger than the radius, an anomaly is detected. Otherwise, the system is still running normally (see Figure 3Right).

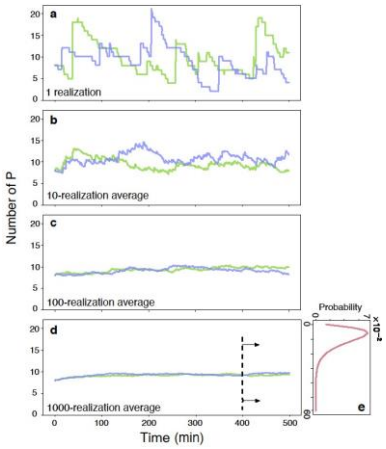

Figure 4: Stochastic simulations for Example 1.

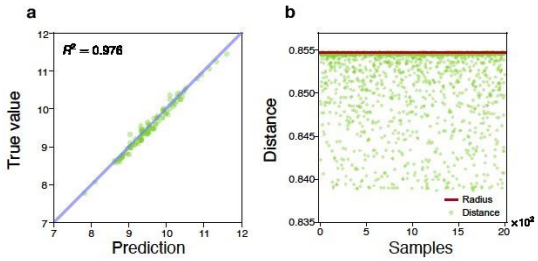

Figure 5: DKNN process monitoring for Example 1 based on mean-value data. (a) shows the DKNN model based on mean-value data cast precise one-step predictions, as predictions (green dots) are close to the line $y = x$ (purple). (b) SVDD calculates the radius (red) for anomaly detection and most samples (green dots) are contained within the radius.

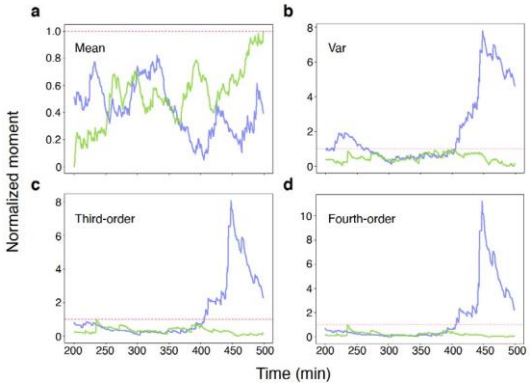

Figure 6: Sensitivity of moments against anomaly. The anomaly occurs at time $t = 401$. All the moments are normalized for visual convenience, and the normalization methods are stated in Appendix 6.2. Moments of order higher or equal to 2 are sensitive to anomaly, while the mean value is not.

Table 1: Anomaly detection F-scores test result for mean-valued data of example 1.

Confidence	90%

Klover Multidisciplinary Journal of Engineering
Volume 10 Issue 1, January-March 2022
ISSN: 2995-4118
Impact Factor: 6.40
http://kloverjournals.org/journals/index.php/Engineering

Time (min)	401	420	450	480
F-score (%)	15.365	11.645	14.155	12.744

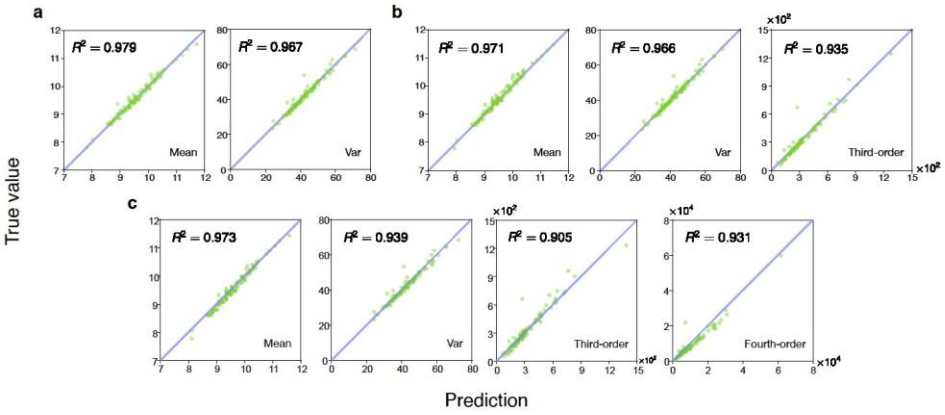

Figure 7: Accuracy of DKNN models one-step prediction for different orders of moments. DKNN model trained on a dataset containing (a) mean and variance; (b) mean, variance and third-order moment; (c) mean, variance, third-order moment and fourth-order moment.

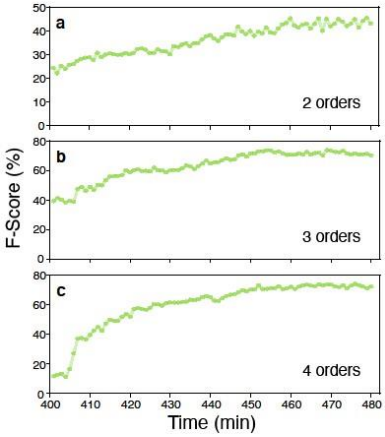

Figure 8: F-score of temporal anomaly detection of three DKNN model trained on dataset containing moments of order up to 2, 3 and 4.

4. Results

Next we unfold the process monitoring protocols on two canonical examples with both firmly rooted in SPS.

4.1. Example 1

The first canonical example considered comprises the following set of biochemical reactions:

$$\varnothing \xrightarrow{\frac{\alpha\beta^i}{(1+\beta)^{i+1}}} iP, \qquad P \xrightarrow{d} \varnothing, \tag{14}$$

where P stands for a protein of interest. The first reaction in (14) in fact represent a group of reactions, and means that the protein is produced in bursts, whose size i conforms to a geometric distribution parametrized by $1/(1+\beta)$, while the second stands for the degradation of protein or its loss of

functionality. The system (14) is known as bursty system in literature, and was found to adequately characterize the stochastic dynamics of most genes in mammalian or human cells [40]. The burst frequency α is selected as 0.0282 min^{-1}, the mean burst size β is 3.46, and the degradation rate constant d is 0.01 min^{-1}. These kinetic parameters correspond to those associated with gene Nanog in mouse embryonic stem cells [40].

We first simulate the system (14) by means of SSA for 1, 10, 100 and 1000 realizations and each for two sets. In either set, the protein numbers are averaged for all realizations at each time point. The results in Figure 4 show that the single-realization data is remarkably noisy and thus poses challenges for establishing a robust process monitoring model (see Figure 4a). The distribution of protein numbers at $t = 400$ min is shown in Figure 4e, and is indeed a negative binomial distribution [40]. The fluctuations are substantially attenuated as the number of averaged realizations increase (see Figures. 4b, 4c, 4d). It suggests that ensemble method is a simple but effective approach for data curation. However, precautions should be taken for large number of realizations for two reasons: (i) the anomaly may be averaged out so that its detection becomes challenging; (ii) the large number of realizations is tantamount to that of cells, whose sampling may be difficult in practice. Here we choose the number to be 100.

Next we show that the mean is not adequate for process monitoring on SPS. To this end, we simulate a fault by decreasing α to a third ($\alpha = 0.0094$ min^{-1}) and increasing β by three times ($\beta = 10.38$) at time $t = 401$. First, we trained a DKNN model with mean values at two successive time points as input and output. The training dataset comprises 2000 data points collected at time $t = 400$ and $t = 401$ corresponding to the steady state (see Figure 4e), while a test set is of size 100, on which an accuracy test is performed. The accuracy of the trained DKNN model is shown in Figure 5a. The predictions are distributed close to the line $y = x$, indicating that these predictions are accurate. By means of SVDD, a radius for anomaly detection is computed and shown as red line in Figure 5b. Most of the residues (~ 90%) are contained within this radius. Within the help of the DKNN model and the radius, we perform the test to detect the aforementioned anomaly occurring at time $t = 401$. The F-scores averaged over 20 independent ensemble samples at 4 different time points are presented in Table 1. It clearly shows that the detection accuracy is low and cannot be improved over time, thereby solidly advocating our statement that mean value is not sufficient for SPS process monitoring. The unsatisfactory result is attributed to the anomaly we specially chose. As stated previously, the steady state distribution of the system (14) is negative binomial parametrized as $\mathrm{NB}(\frac{\alpha}{d}, \frac{1}{1+\beta})$ with the mean being $\alpha\beta/d$. The mean is not altered for the specially selected anomaly. Hence, it is a vivid example showing that the mean value is not adequate to characterize the SPS dynamics and calls for high-order moments. It is also evidenced by Figure 6a that the difference between the faulted and normal trajectories can hardly be discerned, whereas Figures. 6b, 6c, 6d show that high-order moments are much more sensitive to the anomalies. Given the observation, it is necessary to incorporate high-order moments in datasets for SPS anomaly detection. As such, we create another three pairs of training and test datasets, and each has the moments up to order 2, 3 and 4 respectively. The methods of moments calculation are stated in Appendix 6.1. After training DKNN models on the three training datasets, three independent accuracy

Klover Multidisciplinary Journal of Engineering
Volume 10 Issue 1, January-March 2022
ISSN: 2995-4118
Impact Factor: 6.40
http://kloverjournals.org/journals/index.php/Engineering

tests on the corresponding test dataset are carried out, and the results are shown in Figure 7. It shows that the accuracy R^2 degrades as the order of moment of prediction interest increases as expected. Generally, the
fluctuations in higher-order moments are more intense than that in lower-order moments.
Subsequently, we use the three well-trained DKNN models to detect the aforementioned anomaly. It shows in Figure 8 that the detection becomes more accurate as the anomaly effects accumulate in time. Besides, the models based on moments of order 3 and order 4 outperform that of order 2, while the performance of the former two are comparable. Hence, it is concluded that the combination of moments of order up to 3 probably suits best for DKNN model performing anomaly detection in SPS.
Furthermore, we compare the DKNN model and DMD model both trained on the dataset containing moments of order up to 3. The accuracy comparison is summarized in Figure 9a. It shows that DKNN outperforms DMD on the predictions of all the moments. However, the DKNN's advantage is mitigating as the stochasticity gets stronger in higher-order moment data. As for anomaly detection, the F-scores of DKNN are higher than that of DMD by 15% ~ 50% (see Figure 9b).

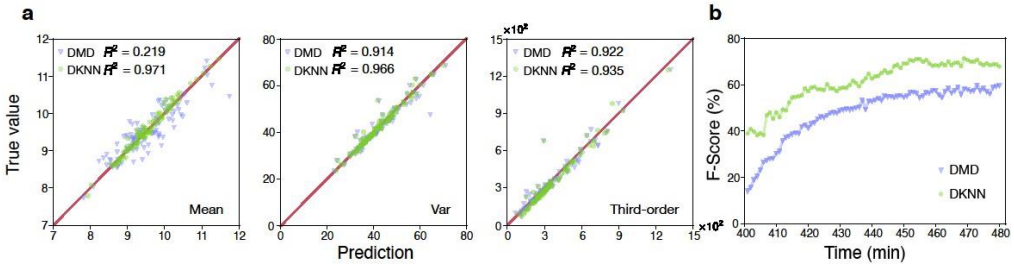

Figure 9: Comparison of DKNN and DMD on (a) prediction accuracy and (b) anomaly detection of Example 1.

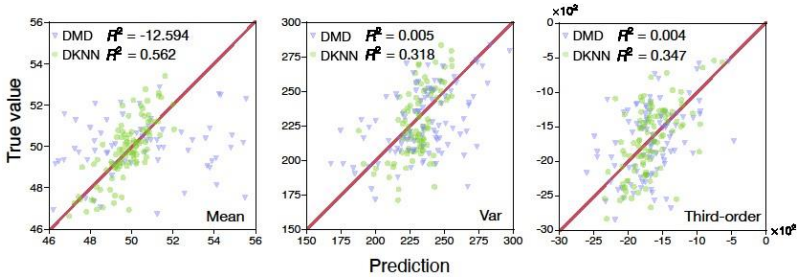

Figure 10: Comparison of DKNN and DMD on prediction accuracy of Example 2.

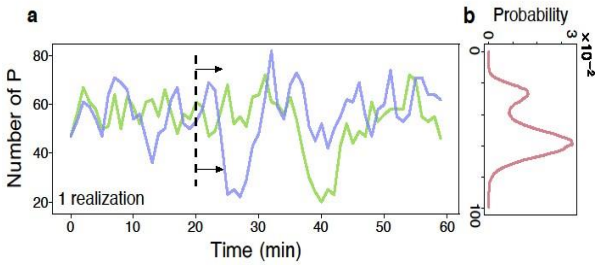

Figure 11: Stochastic simulations for Example 2.
Table 2: Comparision of DKNN and DMD on detection of anomalies case 1 & case 2 in example 2

Klover Multidisciplinary Journal of Engineering
Volume 10 Issue 1, January-March 2022
ISSN: 2995-4118
Impact Factor: 6.40
http://kloverjournals.org/journals/index.php/Engineering

Case	Case 1		Case 2	
Method	DKNN	DMD	DKNN	DMD
Time (min)	21	21	21	21
F-score (%)	92.44	66.67	23.91	16.39

Table 3: DKNN technical details

Case	Case 1		Case 2	
Method	DKNN	DMD	DKNN	DMD
Time (min)	21	21	21	21
F-score (%)	92.44	66.67	23.91	16.39

4.2. Example 2

Next we consider a more complicated example, which is of great biological interest as well. The SPS consists of five biochemical reactions:

$$G \xrightarrow{\rho_1} G + P, \quad G^* \xrightarrow{\rho_2} G^* + P, \quad P \xrightarrow{d} \varnothing,$$
$$G \xrightarrow{\sigma_b} G^*, \quad G^* \xrightarrow{\sigma_u} G. \tag{15}$$

The system as a whole is named telegraph model, which is a renowned model for gene expression in [44]. The symbols G and G^* stand for two gene states that are actively expressing proteins (usually referred as ON state) and less active (referred as OFF state with leakage). The first two reactions in (15) mean protein P being expressed, the third stands for protein degradation, the fourth and fifth mean that the gene is hopping between ON and OFF states. The kinetic parameters we use here are: $\rho_1 = 60\ \text{min}^{-1}$, $\rho_2 = 25\ \text{min}^{-1}$, $d = 1\ \text{min}^{-1}$, $\sigma_b = 0.1\ \text{min}^{-1}$, $\sigma_u = 0.25\ \text{min}^{-1}$. By using SSA, we collect data at time $t = 20, 21$ min to create a training dataset of size 2000 and a test dataset of size 100. Both datasets contain the moments of order up to 3. By training DKNN and DMD model on the training dataset and comparing both on the test dataset, it is found in Figure 10 that DKNN is remarkably better than DMD for predicting all the moments, despite a loss in accuracy compared to the result of Example 1. However, it is with expectation, since the distribution for the kinetic parameters selected is bimodal suggesting the protein number is fluctuating between two disparate levels (see Figure 11). In the following, we further compare both models on detecting two different types of anomalies.

4.2.1. Case 1

The rate ρ_1 is changed to 40 at time $t = 21$ min, which corresponds to gene expression process of state ON changed. Based on the yielded models and the associated residues, SVDD computes the radii of 90% confidence interval for anomaly detection. The detection result is reported in Table 2, where the Fscores strongly support the superiority of DKNN.

4.2.2. Case 2

The rate σ_u is changed to 0.1 at time $t = 21$ min, which corresponds the gene is more often switching to OFF state. By applying the same process monitoring protocol again, the results in Table 2 again confirms DKNN's supremacy against DMD. However, the F-scores are lower than that of Case 1. It may be related to that Case 2 corresponds to a perturbation on the upstream of gene expression, while Case 1 corresponds to the downstream. The upstream perturbation may be buffered by a multitude of downstream processes, and thus becomes more challenging to detect. Nevertheless, Case 2 provides an excellent arena for benchmarking various process monitoring methods.

5. Conclusions

In this paper, we discuss the process monitoring for SPS and develop an integrated method of Koopman operator theory and deep neural network to solve it. The method uses a deep autoencoder structure to establish a bijective mapping between original space and a high-dimensional linear space, where the Koopman operator operates. An anomaly detection threshold is computed by SVDD on the basis of unmodeled residues. It is also argued that given the novel type of stochasticity□—intrinsic noise, the SPS in the form of biochemical systems simulated by SSA can serve as an excellent arena for benchmarking various process monitoring methods. As SPS data is remarkably noisy, we propose to use ensemble method to tackle it and conclude that high-order moments have to be incorporated for robustness.

6. Appendix

6.1. Moment calculation

The moments in data are calculated as central moments

$$S^k = \frac{1}{n-1}\sum_{i=1}^{n}(X_i - \overline{X})^k, \quad (16)$$

where n is the number of samples, X_i stands for the value of sample at a certain time, and $\overline{X}$ is the mean of sample.

6.2. Moment normalization

The moments in the normal case is normalized by the min-max method as follows

$$X_{norm} = \frac{X - X_{min}}{X_{max} - X_{min}}, \quad (17)$$

where X is the raw moment data, X_{norm} stands for the normalized moment, and X_{min}, X_{max} stand for the minimum and maximum of the raw data. The moments in the faulted case are normalized as per the minimum X_{min} and maximum X_{max} of the normal case.

6.3. Neural network details

The Koopman operator is implemented as a linear network. All the technical details of DKNN including network structure and hyperparameters are summarized in Table 3. All the weights of neural network are initialized as per a truncated normal distribution $\mathcal{N}(0, 0.1)$, while the biases are set to 0. The training optimizer is Adam with a learning rate equal to 0.001.

References

Wang, G., Haringa, C., Noorman, H., Chu, J., and Zhuang, Y. (2020). Developing a Computational Framework to Advance Bioprocess Scale-Up. Trends in Biotechnology, 38(8), 846-856.

Lu, J., Cao, Z., Zhao, C., and Gao, F. (2019). 110th Anniversary: An Overview on Learning-Based Model Predictive Control for Batch Processes. Industrial & Engineering Chemistry Research, 58(37), 17164-17173.

Jiang, Q., Wang, Z., Yan, S., and Cao, Z. (2022). Data-Driven Soft Sensing for Batch Processes Using Neural Network-Based Deep Quality-Relevant Representation Learning. IEEE Transactions on Artificial Intelligence.

Cao, Z., Yu, J., Wang, W., Lu, H., Xia, X., Xu, H., and Zhang, L. (2020). Multi-Scale Data-Driven Engineering for Biosynthetic Titer Improvement. Current Opinion in Biotechnology, 65, 205-212. [5] Gao, J., Feng, E., and Zhang, W. (2022). Modeling and Parameter Identification of Microbial Batch Fermentation under Environmental Disturbances. Applied Mathematical Modelling, 108, 205-219.

Soukoulis, C., Panagiotidis, P., Koureli, R., and Tzia, C. (2007). Industrial Yogurt Manufacture: Monitoring of Fermentation Process and Improvement of Final Product Quality. Journal of dairy science, 90(6), 2641-2654.

Sriramula, S., and Chryssanthopoulos, M. K. (2009). Quantification of Uncertainty Modelling in Stochastic Analysis of FRP Composites. Composites Part A: Applied Science and Manufacturing, 40(11), 1673-1684.

Lu, H., Plataniotis, K. N., and Venetsanopoulos, A. N. (2008). MPCA: Multilinear Principal Component Analysis of Tensor Objects. IEEE transactions on Neural Networks, 19(1), 18-39. [9] Lee, J. M., Yoo, C., and Lee, I. B. (2004). Fault Detection of Batch Processes Using Multiway Kernel Principal Component Analysis. Computers & Chemical Engineering, 28(9), 1837-1847.

Jia, Z. Y., Wang, P., and Gao, X. J. (2012). Process Monitoring and Fault Diagnosis of Penicillin Fermentation Based on Improved MICA. Advanced Materials Research, 591, 1783-1788.

Zhao, C., Gao, F., and Wang, F. (2009). Nonlinear Batch Process Monitoring Using Phase-Based Kernel-Independent Component Analysis–Principal Component Analysis (KICA–PCA). Industrial & Engineering Chemistry Research, 48(20), 9163-9174.

Peng, C., Chunhao, D., and Qiankun, Z. (2020). Fault Diagnosis of Microbial Pharmaceutical Fermentation Process with Non-Gaussian and Nonlinear Coexistence. Chemometrics and Intelligent Laboratory Systems, 199, 103931.

Yang, C., and Hou, J. (2016). Fed-Batch Fermentation Penicillin Process Fault Diagnosis and Detection Based on Support Vector Machine. Neurocomputing, 190, 117-123.

Ding, J., Cao, Y., Mpofu, E., and Shi, Z. (2012). A Hybrid Support Vector Machine and Fuzzy Reasoning Based Fault Diagnosis and Rescue System for Stable Glutamate Fermentation. Chemical Engineering Research and Design, 90(9), 1197-1207.

Hornik, K., Stinchcombe, M., and White, H. (1989). Multilayer Feedforward Networks Are Universal Approximators. Neural Networks, 2(5), 359-366.

Shimizu, H., Yasuoka, K., Uchiyama, K., and Shioya, S. (1997). On-Line Fault Diagnosis for Optimal Rice a-Amylase Production Process of a Temperature-Sensitive Mutant of Saccharomyces Cerevisiae by an Autoassociative Neural Network. Journal of Fermentation and Bioengineering, 83(5), 435-442.

Lopes, J. A., and Menezes, J. C. (2004). Multivariate Monitoring of Fermentation Processes with Non-Linear Modelling Methods. Analytica Chimica Acta, 515(1), 101-108.

Yu, J., Zhang, C., and Wang, S. (2021). Multichannel One-Dimensional Convolutional Neural Network-Based Feature Learning for Fault Diagnosis of Industrial Processes. Neural Computing and Applications, 33, 3085-3104.

Chen, S., Yu, J., and Wang, S. (2020). One-Dimensional Convolutional Auto-Encoder-Based Feature Learning for Fault Diagnosis of Multivariate Processes. Journal of Process Control, 87, 54-67. [20] Peng, C., Lu, R., Kang, O., and Kai, W. (2020). Batch Process Fault Detection for Multi-Stage Broad Learning System. Neural Networks, 129, 298-312.

Chen, H., Liu, Z., Alippi, C., Huang, B., and Liu, D. (2022). Explainable Intelligent Fault Diagnosis for Nonlinear Dynamic Systems: From Unsupervised to Supervised Learning. IEEE Transactions on Neural Networks and Learning Systems.

Chen, H., Chai, Z., Dogru, O., Jiang, B., and Huang, B. (2021). Data-Driven Designs of Fault Detection Systems Via Neural Network-Aided Learning. IEEE Transactions on Neural Networks and Learning Systems, 33(10), 5694-5705.

Sherstinsky, A. (2020). Fundamentals of Recurrent Neural Network (RNN) and Long Short-Term Memory (LSTM) Network. Physica D: Nonlinear Phenomena, 404, 132306.

Zhang, M., Li, X., and Wang, R. (2021). Incipient Fault Diagnosis of Batch Process Based on Deep Time Series Feature Extraction. Arabian Journal for Science and Engineering, 1-12.

Ren, J., and Ni, D. (2020). A Batch-Wise LSTM-Encoder Decoder Network for Batch Process Monitoring. Chemical Engineering Research and Design, 164, 102-112.

Koopman, B. O. (1931). Hamiltonian Systems and Transformation in Hilbert Space. Proceedings of the National Academy of Sciences, 17(5), 315-318.

Brunton, S. L. (2019). Notes on Koopman Operator Theory. Universität Von Washington, Department of Mechanical Engineering, Zugriff, 30.

Rowley, C. W., Mezić, I., Bagheri, S., Schlatter, P., and Henningson, D. S. (2009). Spectral Analysis of Nonlinear Flows. Journal of Fluid Mechanics, 641, 115-127.

Schmid, P. J. (2010). Dynamic Mode Decomposition of Numerical and Experimental Data. Journal of Fluid Mechanics, 656, 5-28.

Williams, M. O., Kevrekidis, I. G., and Rowley, C. W. (2015). A Data–Driven Approximation of the Koopman Operator: Extending Dynamic Mode Decomposition. Journal of Nonlinear Science, 25, 13071346.

Korda, M., and Mezić, I. (2018). Linear Predictors for Nonlinear Dynamical Systems: Koopman Operator Meets Model Predictive Control. Automatica, 93, 149-160.

Brunton, S. L., Brunton, B. W., Proctor, J. L., and Kutz, J. N. (2016). Koopman Invariant Subspaces and Finite Linear Representations of Nonlinear Dynamical Systems for Control. Plos One, 11(2), e0150171.

Lusch, B., Kutz, J. N., and Brunton, S. L. (2018). Deep Learning for Universal Linear Embeddings of Nonlinear Dynamics. Nature Communications, 9(1), 4950.

Yeung, E., Kundu, S., and Hodas, N. (2019, July). Learning Deep Neural Network Representations for Koopman Operators of Nonlinear Dynamical Systems. In 2019 American Control Conference (ACC) (pp. 4832-4839). IEEE.

Dubey, R., Samantaray, S. R., Panigrahi, B. K., and Venkoparao, V. G. (2016). Koopman Analysis Based Wide-Area Back-Up Protection and Faulted Line Identification for Series-Compensated Power Network. IEEE Systems Journal, 12(3), 2634-2644.

Dang, Z., Lv, Y., Li, Y., and Wei, G. (2018). Improved Dynamic Mode Decomposition and Its Application to Fault Diagnosis of Rolling Bearing. Sensors, 18(6), 1972.

Cheng, C., Ding, J., and Zhang, Y. (2020). A Koopman Operator Approach for Machinery Health Monitoring and Prediction with Noisy and Low-Dimensional Industrial Time Series. Neurocomputing, 406, 204-214.

Liu, B., Xiao, Y., Cao, L., Hao, Z., and Deng, F. (2013). Svdd-Based Outlier Detection on Uncertain Data. Knowledge and Information Systems, 34, 597-618.

Larsson, A. J., Johnsson, P., Hagemann-Jensen, M., Hartmanis, L., Faridani, O. R., Reinius, B., and Sandberg, R. (2019). Genomic Encoding of Transcriptional Burst Kinetics. Nature, 565(7738), 251254.

Cao, Z., and Grima, R. (2020). Analytical Distributions for Detailed Models of Stochastic Gene Expression in Eukaryotic Cells. Proceedings of the National Academy of Sciences, 117(9), 4682-4692. [41] Gillespie, D. T. (1977). Exact Stochastic Simulation of Coupled Chemical Reactions. The Journal of Physical Chemistry, 81(25), 2340-2361.

Fu, X., Zhou, X., Gu, D., Cao, Z., and Grima, R. (2022). DelaySSAToolkit. jl: Stochastic Simulation of Reaction Systems with Time Delays in Julia. Bioinformatics, 38(17), 4243-4245.

Brunton, S. L., Budišić, M., Kaiser, E., and Kutz, J. N. (2021). Modern Koopman Theory for Dynamical Systems. arXiv preprint arXiv:2102.12086.

Cao, Z., and Grima, R. (2018). Linear Mapping Approximation of Gene Regulatory Networks with Stochastic Dynamics. Nature Communications, 9(1), 3305.